Acta Crystallographica Section D
Biological Crystallography
ISSN 0907-4449

Dwelling in the dark: procedures for the crystallography of phytochromes and other photochromic proteins

Jo Mailliet,[a]‡ Georgios Psakis,[a]‡ Claudia Schroeder,[b] Sabine Kaltofen,[a] Ulrike Dürrwang,[a] Jon Hughes[a]* and Lars-Oliver Essen[b]*

[a]Justus Liebig University Giessen, Plant Physiology, Senckenbergstrasse 3, D-35390 Giessen, Germany, and [b]Philipps University Marburg, Structural Biochemistry, Hans-Meerwein-Strasse, D-35032 Marburg, Germany

‡ These authors contributed equally to this work.

Correspondence e-mail: jon.hughes@uni-giessen.de, essen@staff.uni-marburg.de

Received 14 July 2009
Accepted 25 August 2009

Crystallization of phytochromes and other photochromic proteins is hampered by the conformational changes that they undergo on exposure to light. As a canonical phytochrome, cyanobacterial Cph1 switches between two stable states upon absorption of red/far-red light. Consequently, it is mandatory to work in darkness from protein purification to crystal cryoprotection in order to ensure complete occupancy of one state or the other. With the simple and inexpensive methods that have been developed, phytochromes and other photochromic molecules can effectively be handled and crystallized, as has been demonstrated by the solution of the three-dimensional structure of the Cph1 sensory module.

1. Introduction

Phytochromes are red/far-red absorbing photoreceptors that form two (meta-)stable but interconvertible photochromic states (Pr and Pfr) with λ_{max} of ~650–670 and ~705–730 nm, respectively. Initial insights into the structure of phytochromes were obtained from the PAS-GAF bidomain of *Deinococcus radiodurans* bacteriophytochrome (PDB code 1ztu; Wagner *et al.*, 2005). Recently, however, we were able to solve the structure of the complete photochromically competent sensory module (Cph1Δ2) of the cyanobacterial phytochrome Cph1 from *Synechocystis* 6803 (PDB code 2vea; Essen *et al.*, 2008). Cph1 (Hughes *et al.*, 1997; Yeh *et al.*, 1997) is a valuable model for phytochrome studies because the sensory module closely resembles that of plant phytochromes and can be purified to homogeneity as either Pr or Pfr (Strauss *et al.*, 2005; Zeidler *et al.*, 2006). Moreover, as a photon-switchable sensory histidine protein kinase, full-length Cph1 allows in-depth investigations of two-component signalling mechanisms. However, its sensitivity to light presents a challenge for biochemical handling, crystallization and crystal mounting. Here, we describe simple but effective methods for handling phytochromes and elucidate the consequences arising from light exposure at any stage from purification to X-ray diffraction measurements of Cph1Δ2 crystals.

2. Materials and methods

2.1. Sample preparation

Recombinant overproduction/purification of Cph1Δ2 assembled with its cognate phycocyanobilin (PCB) chromophore was performed as described previously (Essen *et al.*, 2008; Hahn *et al.*, 2006; Landgraf *et al.*, 2001). The sample was irradiated in a 250 µl Hamilton syringe with saturating far-red light (λ_{max} = 730 ± 20 nm) to achieve greater than 99% occupancy of the Pr state. However, the situation for Pfr is more difficult. As Pfr absorbs strongly at the Pr λ_{max}, the highest occupancy obtainable for Pfr is ~70% (Lamparter *et al.*, 1997; van Thor *et al.*, 2001). However, we discovered that Pfr dimers are about 20-fold more stable than those of Pr (Strauss *et al.*, 2005), thus allowing the preparation of Pfr at near 100% occupancy by size-exclusion chromatography (SEC) using a protein concentration of 3–5 mg ml^{-1} at which the Pr state of Cph1Δ2 is monomeric but Pfr is largely dimeric.

All procedures were carried out either under very weak blue–green safelight (λ_{max} = 490 ± 20 nm) or under below-red conditions (IR), as described below.

2.2. IR visualization

An Olympus SZ60 microscope equipped with 20× oculars was modified for IR visualization. The standard halogen lamp was replaced by a single IR LED (λ_{max} = 940 ± 45 nm; Roithner Optics, Vienna, Austria) driven by an adjustable stabilized-current power supply. Additional moveable LEDs were provided for top IR illumination. Adapters for the microscope oculars (Figs. 1*c* and 1*d*) accommodated a pair of miniature CCD video cameras (#190974, Conrad Electronic, Germany). CCD sensors have a λ_{max} of 0.9–1.1 µm and the camera used had a particularly high sensitivity on account of its f1.2 aperture. The paired video signals were fed to a head-mounted visor display (3-Scope; Trivisio Prototyping, Frankfurt am Main, Germany), allowing macrostereoscopic visualization for screening, handling and mounting of crystals under IR. To enable other procedures to also be carried out under IR, the video signal was switchable to a single CCD camera mounted on the visor itself and LED-array IR sources were positioned around the work area. The setup is shown in Fig. 1(*d*).

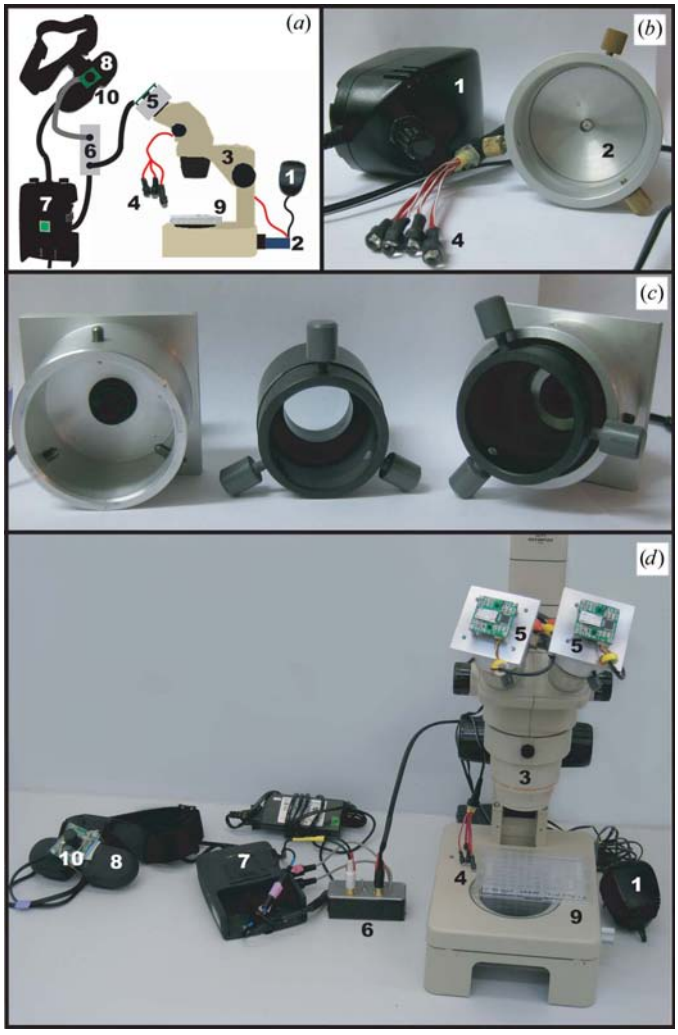

Figure 1
IR stereomicroscope setup used for crystal screening, mounting and freezing in darkness. (*a*) Schematic view. (*b*) Power supply (1) and IR sources (2 and 4). (*c*) CCD camera adapters. (*d*) Overall setup. A variable power unit (1) supplies constant current to an IR LED (2) mounted in place of the halogen lamp of a conventional zoom stereomicroscope (3). Separate LEDs (4) provide top IR illumination of the sample. Paired CCD video cameras are mounted on the oculars (5). The video signals are routed *via* a switch (6) to the converter (7) feeding the visor headpiece (8), allowing stereoscopic observation and handling of crystals in the crystal plate (9). A third CCD camera (10) attached to the visor provides an alternative monoscopic view of the working environment.

2.3. Crystallization and data collection

Crystallization screens were carried out using the sitting-drop vapour-diffusion method in 96-well Greiner plates. Blue-green tetragonal crystals appeared in 2.5 *M* sodium acetate and 0.1 *M* sodium acetate pH 4.6 (Anions Suite, Qiagen) after one week of incubation at 291 K in darkness and reached full size after three weeks. Further optimization was performed in 96-well Greiner plates and/or 24-well plates using hanging-drop vapour diffusion by varying the pH of the buffer, the precipitant concentration and by exchanging the sodium ions for different monovalent or divalent cations. Optimal diffraction was achieved with a 200 × 100 µm tetragonal crystal (space group $P4_32_12$) from 2 *M* sodium acetate/0.1 *M* magnesium acetate pH 5.0. Crystallization procedures and crystal observations were initially performed under blue–green safelight conditions and subsequently using the IR setup (Fig. 1). Diffraction patterns were recorded on beamlines X-13/BW7A and ID14-3 at EMBL Hamburg and ESRF Grenoble, respectively. Flash cryo-annealing was performed in darkness (Yeh & Hol, 1998). Images were collected at $\varphi = 0^\circ$ and $\varphi = 90^\circ$ with 0.5° oscillations at 100 K before and after cryo-annealing.

2.4. UV–Vis spectroscopy

Absorbance spectra in solution were recorded using a modified Agilent 8453 UV–Vis diode detector-array spectrophotometer (Hahn *et al.*, 2006). Microspectroscopic measurements of protein crystals were performed at the ESRF cryobench (Bourgeois *et al.*, 2002). Crystals were irradiated with 532 nm (24 mW, NG-11010-110, JDS Uniphase) or 632 nm (10 mW, GLG 5410, NEC) lasers. The crystals were rotated for 5–10 s on the goniometer during illumination.

3. Results and discussion

3.1. Phytochrome sample preparation

For protein crystallization, it is essential to isolate a monodisperse quaternary state of the molecule and to separate native monomeric or dimeric species from misfolded aggregates. In the case of Cph1 and other photochromic photoreceptors, the photoactive states (Pr/Pfr) have to be obtained at full occupancy, requiring handling procedures which are photodynamically innocuous. Following complete photoconversion to Pr by actinic far-red light, the minimum concentration required for complete dimerization of Pr was >10 mg ml^{-1}. To obtain pure Pfr preparations the concentration was adjusted to 5 mg ml^{-1}, at which Pfr eluted as a dimer while Pr remained monomeric (Strauss *et al.*, 2005). The apparent molecular mass of the Cph1Δ2 dimers was 110 kDa, with the shoulder at 69 kDa corresponding to misfolded apoprotein unable to bind PCB (SEC; Supplementary Fig. 1*a*[1]). Coomassie-stained SDS–PAGE gels (Supplementary Fig. 1*b*[1]) showed a purity of approximately 75% after Ni^{2+}-affinity purification and almost 99% purity after SEC. The 660/280 nm specific absorbance ratio (SAR) after SEC was 1.3, indicating 100% purity

[1] Supplementary material has been deposited in the IUCr electronic archive (Reference: MH5030). Services for accessing this material are described at the back of the journal.

(Lamparter *et al.*, 2001). Zinc acetate staining (Berkelman & Lagarias, 1986) confirmed covalent PCB binding to Cph1Δ2 (Supplementary Fig. 1*c*).

3.2. Initial phytochrome crystal handling

Cryoprotection of Cph1Δ2 crystals under white light with 20% glycerol only resulted in poor crystal diffraction (4–6 Å resolution; Supplementary Table 1) and systematic formation of ice rings (data not shown). The quality of diffraction did not improve even when the percentage of glycerol was increased to 40%. Only when the crystals were thawed and partly dried in air for ∼15–30 s before refreezing was an improvement of diffraction observed (the best native crystal showed anisotropic diffraction of 2.8 × 2.8 × 3.45 Å). However, this method proved to be poorly reproducible and failed with the SeMet-labelled Cph1Δ2 crystals.

3.3. Handling after optimization and use of IR equipment

Following the unsatisfactory diffraction of glycerol-protected crystals, we attempted optimization of the original condition by using acetate salts at various concentrations (overall pH 6.6–7.2) in darkness. Crystals grown with 0.1 *M* ammonium or calcium acetate did not show better diffraction, whereas 0.1 *M* magnesium acetate together with 2 *M* sodium acetate (overall pH 6.7) yielded the best diffracting crystals (Essen *et al.*, 2008). Thus, for cryoprotection the crystal-

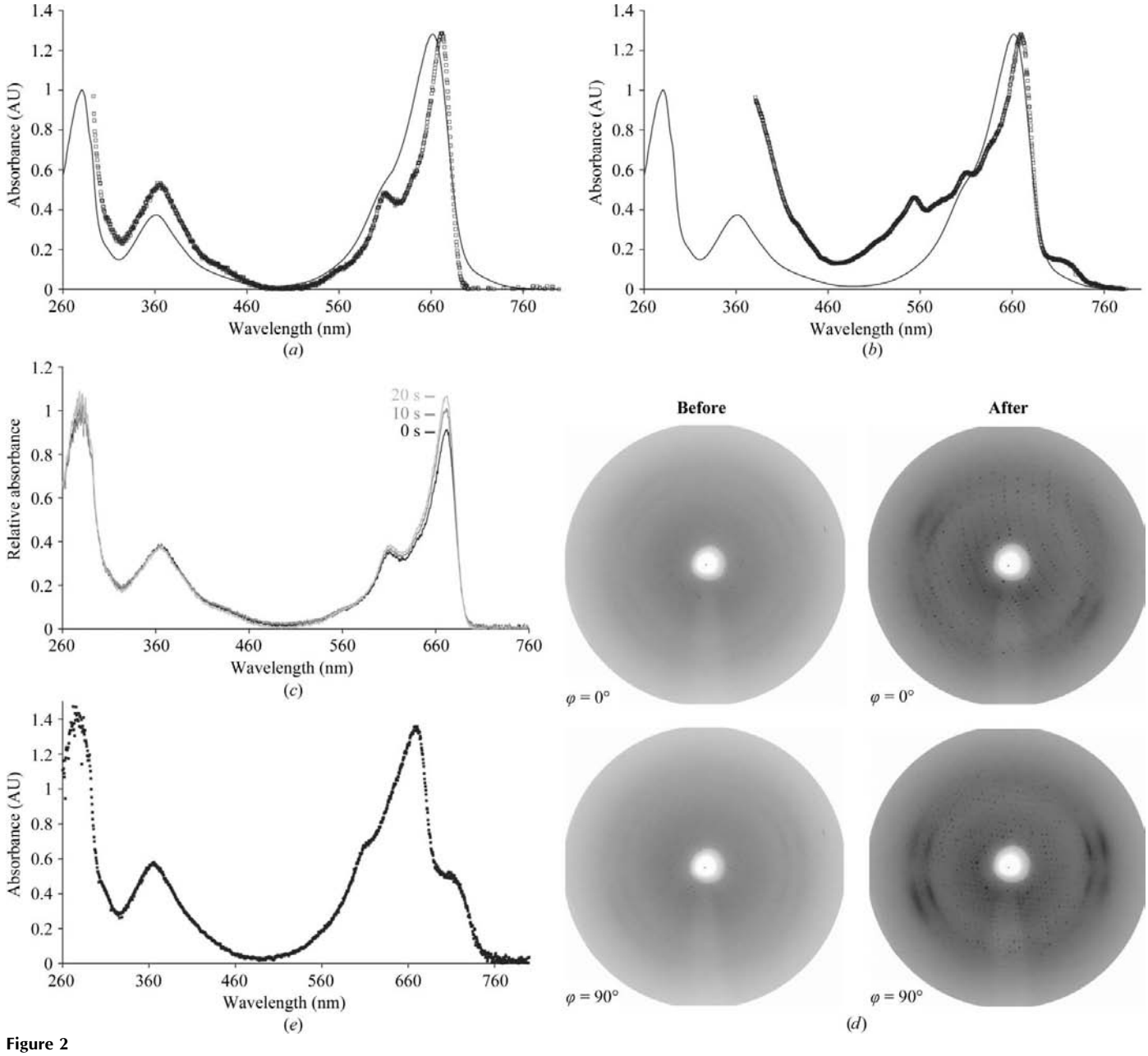

Figure 2
Absorbance spectra of the Pr state of Cph1Δ2 in solution (dashed lines) and in the crystalline form (squares) and X-ray diffraction patterns. (*a*) Spectrum of crystals harvested from 1.8 *M* sodium acetate and 0.1 *M* sodium acetate pH 4.6 (overall pH 6.5) recorded before X-ray irradiation. (*b*) Spectrum of crystals harvested from 2.3 *M* sodium acetate and 0.1 *M* sodium acetate pH 4.4 (overall pH 6.5) recorded after 18 h X-ray irradiation at beamline X-13 (EMBL Hamburg). (*c*) Spectrum of crystals prior to cryo-annealing, after 10 s cryo-annealing and after 20 s cryo-annealing in darkness. (*d*) Diffraction patterns prior to and after cryo-annealing recorded on beamline BW7A (EMBL Hamburg). (*e*) Absorbance spectrum of Cph1Δ2 crystals exposed to white light prior to freezing.

lization buffer was supplemented with 25% magnesium acetate (Rubinson *et al.*, 2000) instead of glycerol. Microspectroscopy of these crystals was difficult on account of the very high concentration and extinction coefficient, with only the smallest crystals yielding spectra in which the λ_{max} peak was resolved. However, these crystals diffracted poorly.

Crystals mounted and cryoprotected under IR light showed a similar absorbance spectrum at 100 K to Cph1Δ2 in solution at 298 K (Fig. 2*a*). Differences included narrowing of the peaks and a 10 nm bathochromic shift of the red λ_{max} band. The absorbance spectrum of the crystal used for data collection after 18 h continuous X-ray irradiation (flux of 3.16×10^{11} photons s^{-1}) showed the Pr peak and a minor peak (715 nm) perhaps representing the Pfr form with a similar bathochromic shift to that observed for Pr (Fig. 2*b*). The occurrence of the Pfr peak might reflect chromophore mobility resulting from radiation damage. Cryo-annealing itself performed in darkness had no significant effect on the absorbance spectra (Fig. 2*c*). Cryoprotection with 25% magnesium acetate in combination with flash cryo-annealing (Yeh & Hol, 1998) considerably improved the diffraction (Fig. 2*d*, Supplementary Table 1), but the previously observed anisotropy remained (maximal resolution $2.7 \times 2.7 \times 2.2$ Å). The overall improved crystal quality facilitated structure solution by MAD (SeMet crystals; 2.8 Å resolution). Exposure of the crystals to white light prior to freezing resulted in partial photoconversion (Fig. 2*e*) but unfortunately almost complete loss of diffraction. The same effect was also observed when crystals that had been picked up and frozen under IR were irradiated at 293 K with an intense red laser (Essen *et al.*, 2008). We attribute this to the disturbance of the crystal contacts between the tongue region of the PHY domain (Essen *et al.*, 2008) and the C-terminal histidine tag of Cph1Δ2 as a consequence of photoconversion. IR irradiation itself at room temperature induced no photoconversion and had no effect on diffraction.

In summary, our procedures enabled the successful purification, crystallization and three-dimensional structural solution of the monodisperse Cph1 sensory module. The success of this work relied on the use of an IR stereomicroscope for visualization and manipulation of the photosensitive crystals in darkness. Any commercially available stereomicroscope can be successfully adapted for use with IR in the manner we describe. Crystal screening, mounting and cryoprotection in the dark would have been impossible without the use of the stereoscopic video headset connected to the IR microscope. We also demonstrated the effects of white light on the spectral and diffraction behaviour of Cph1Δ2 crystals and showed how the use of IR imaging and optimized cryobuffer and cryo-annealing conditions are critical for obtaining crystals of good diffraction quality. The current setup provides an invaluable tool for any laboratory wishing to characterize photoreceptors existing in different light-dependent conformations.

This work was supported by DFG grants HU702/6 to JH and ES152/6-1 to L-OE. The authors are grateful for the support by Andrea Schmidt at synchrotron beamline X-13, EMBL, Hamburg, by Stephanie Monaco at ESRF beamline ID14-3, Grenoble and for the technical support provided by Werner Kröschel, Tina Lang and Petra Gnau.

References

Berkelman, T. R. & Lagarias, J. C. (1986). *Anal. Biochem.* **156**, 194–201.
Bourgeois, D., Vernede, X., Adam, V., Fioravanti, E. & Ursby, T. (2002). *J. Appl. Cryst.* **35**, 319–326.
Essen, L.-O., Mailliet, J. & Hughes, J. (2008). *Proc. Natl Acad. Sci. USA*, **105**, 14709–14714.
Hahn, J., Strauss, H. M., Landgraf, F. T., Gimenez, H. F., Lochnit, G., Schmieder, P. & Hughes, J. (2006). *FEBS J.* **273**, 1415–1429.
Hughes, J., Lamparter, T., Mittmann, F., Hartmann, E., Gärtner, W., Wilde, A. & Börner, T. (1997). *Nature (London)*, **386**, 663.
Lamparter, T., Esteban, B. & Hughes, J. (2001). *Eur. J. Biochem.* **268**, 4720–4730.
Lamparter, T., Mittmann, F., Gärtner, W., Börner, T., Hartmann, E. & Hughes, J. (1997). *Proc. Natl Acad. Sci. USA*, **94**, 11792–11797.
Landgraf, F. T., Forreiter, C., Hurtado, P. A., Lamparter, T. & Hughes, J. (2001). *FEBS Lett.* **508**, 459–462.
Rubinson, K. A., Ladner, J. E., Tordova, M. & Gilliland, G. L. (2000). *Acta Cryst.* D**56**, 996–1001.
Strauss, H. M., Schmieder, P. & Hughes, J. (2005). *FEBS Lett.* **18**, 3970–3974.
Thor, J. J. van, Borucki, B., Crielaard, W., Otto, H., Lamparter, T., Hughes, J., Hellingwerf, K. J. & Heyn, M. P. (2001). *Biochemistry*, **40**, 11460–11471.
Wagner, J. R., Brunzelle, J. S., Forest, K. T. & Vierstra, R. D. (2005). *Nature (London)*, **438**, 325–331.
Yeh, J. I. & Hol, W. G. J. (1998). *Acta Cryst.* D**54**, 479–480.
Yeh, K. C., Wu, S. H., Murphy, J. T. & Lagarias, J. C. (1997). *Science*, **277**, 1505–1508.
Zeidler, M., Lang, C., Hahn, J. & Hughes, J. (2006). *Int. J. Biol. Macromol.* **39**, 100–103.